Electrical impedance tomography using level set representation and total variational regularization*

Eric T. Chung†, Tony F. Chan‡ and Xue-Cheng Tai§

November 12, 2003

Abstract

In this paper, we propose a numerical scheme for the identification of piecewise constant conductivity coefficient for a problem arising from electrical impedance tomography. The key feature of the scheme is the use of level set method for the representation of interface between domains with different values of coefficients. Numerical tests show that our method can be able to recover a sharp interface and can tolerate higher level of noise in the observation data. Results concerning the effects of number of measurements, noise level in the data as well as the regularization parameters on the accuracy of the scheme are also given.

1 Introduction

Electrical impedance tomography is a widely investigated problem with many applications in physical and biological sciences. It is well known that the inverse problem is nonlinear and highly ill-posed. Various of numerical techniques with different advantages have been proposed to solve the problem. First of all, we will give a precise mathematical model for electrical impedance tomography. Let Ω be a bounded domain in $\mathbb{R}^2$ with C^1 boundary $\partial\Omega$ having outward normal n. We assume Ω contains material with electrical conductivity $q(x)$ satisfying $q(x) \geq q_0 > 0$. Then the electrical potential $u(x)$ inside Ω satisfies

$$-\nabla \cdot (q\nabla u) = 0 \quad \text{in} \quad \Omega, \tag{1}$$

$$q\frac{\partial u}{\partial n} = f \quad \text{on} \quad \partial\Omega, \tag{2}$$

*We acknowledge support from the ONR under grant N00014-96-1-0277, from the NSF under contract DMS-9973341 and from the NIH under grant P20MH65166.

†Department of Mathematics, University of California, Los Angeles, CA 90095-1555, USA. Email: tschung@math.ucla.edu.

‡Department of Mathematics, University of California, Los Angeles, CA 90095-1555, USA. Email: chan@math.ucla.edu.

§Department of Mathematics, University of Bergen, Johnnes Brunsgate 12, N-5007 Bergen, Norway. Email: tai@mi.uib.no.

where $f(x)$ is applied current density on $\partial\Omega$ such that the following conservation of charge relation holds:

$$\int_{\partial\Omega} f(s)\, ds = 0.$$

The problem of electrical impedance tomography is to determine the electrical conductivity $q(x)$ inside Ω using a set of given values of applied current density $f(x)$ on $\partial\Omega$ and the corresponding values of electrical potential $u(x)$ on $\partial\Omega$. Such a mathematical model is obtained from Maxwell's equation under some conditions. See [10] and [14, 23] for some more deltails about the derivation of the above model.

There are many efficient numerical techniques for solving the inverse problem. For instances, in Cheney, Isaacson, Newell, Goble and Simske [11], a method called NOSER has been proposed. The idea is to minimize the L^2-norm of the difference between the electrical potential due to the applied current and the measured potential on $\partial\Omega$. A one step Newton's method, with constant conductivity as initial guess, is employed to solve the minimization problem. The advantage is that most of the calculations, including the gradient of the functional to be minimized, can be done analytically. So, the reconstruction algorithm is very efficient. As the authors of [11] mentioned, one major drawback of this technique is that the recovered conductivity is not accurate. However, the numerical result is good enough for most real applications. See also Cheney, Isaacson and Johathan [10] for an extensive survey on this method.

In Brühl and Hanke [4], a method, based on an explicit criterion of whether a point is lying inside or outside of a certain set, have been proposed. Thus, a region with certain conductivity value can be reconstructed by testing every point in the computational domain. There is no need to minimize any functional, which means that there is no need to solve the forward problem numerically, as it is required to perform many times when computing the gradient of the corresponding functional. Results of their experiments show that the method produces reasonably accuracy in most cases for noise level up to 1%. A theoretical justification of the numerical scheme has been given in Brühl [3].

Recently, the Mumford-Shah functional was extended to the electrical impedance tomography problem in Rondi and Santosa [22]. In addition to minimizing the L^2-norm of the difference between the potential due to the applied current and the measured potential, the L^2-norm of the gradient of the conductivity outside a discontinuity set and the Hausdorff measure of the discontinuity set are used a penalization terms. The conductivity coefficient is assumed to be known in a narrow region near the domain boundary. With presence of 1% of noise in the data, both of material interface and coefficient values can be accurately recovered. Besides numerical results, theoretical analysis of the numerical scheme is also given in [22]. See also [13, 12, 1, 23] for some related studies for the same problem.

The level set idea, devised in Osher and Sethian [21], is known to be a powerful and versatile tool to model evolution of interfaces. The idea has also been used successfully in the context of inverse problem. The pioneering work of Os-

her and Santosa [20] uses the level set method for an inverse problem associated with shape optimization for the eigenvalues of the Laplace equation. In Ito, Kunisch and Li [16], the idea has been employed to solve an inverse conductivity problem. Assuming known conductivity values, the unknown conductivity interface can be solved by using values of Neumann data as well as values of solution in a thin layer along the boundary of a domain. In Chan and Tai [8], the level set idea has been applied to solve elliptic inverse problems, where the unknown discontinuous coefficient has to be solved without the knowledge of both the values of the coefficient and interfaces between the regions having different coefficient values. By using the value of solution or the gradient of solution of the forward problem in the domain, the coefficient can be accurately identified by utilizing the level set method. In Dorn, Miller and Rappaport [15], level set method has also been applied to solve an electromagnetic tomography problem with the model given by the Helmholtz equation. With known conductivity values, the interfaces of different materials are determined by using level set representation of curves. The work Ameur, Burger and Hackl [2] treats a geometrical inverse problem using the level set methods. They try to recover a crack in side a elasticity body from just one boundary measurement. In [5, 7, 6, 18] for some other algorithms in using level set methods for some inverse problems.

In this paper, we will propose a method based on the level set idea to solve the inverse problem arising from electrical impedance tomography. We will consider the case where the electrical conductivity $q(x)$ is a piecewise constant function, with the possiblity that the conductivity values are unknown. Following Chan and Tai [8, 9] and Vese and Chan [25], we will represent the conductivity by using level set functions. With the representation of $q(x)$, we then solve the inverse problem by minimizing the L^2-norm of the difference between the potential due to the applied current and the measured potential on $\partial\Omega$. Since the minimization problem is highly ill-posed, we introduce a regularization using the total variation norm of $q(x)$ as in [9]. The choice of the regularization term allows the method to recover a sharp interface between different regions having different conductivity values. Moreover, it has been shown numerically that our method can tolerate higher level of noise in the data.

This paper is organised as follows. In section 2, we will give a brief overview of the level set method. We will present the use of level set function to represent a piecewise constant function. Then we will derive our method for solving the tomography problem by minimizing the L^2-error with total variation regularization. In section 3, a series of numerical experiments is presented. We will show numerically that our method is able to recover simutaneously the unknown interface and the coefficient values. Also, we will discuss the sensitivity of our method with respect to number of observations, noise level and regularization parameter. Finally, in the appendix, we will provide, for completeness, a proof for the formula of the gradient of the cost functional.

2 Numerical solutions to the inverse problem

For simplicity of presentation, we assume Ω contains two different materials with piecewise constant conductivities q_1 and q_2 where q_1 and q_2 are two positive real numbers. In light of the mulitple level sets idea in Vese and Chan [25], the following presentation can be easily generalized to the case where the domain contains more than two materials. Let Ω_i be the region containing material with conductivity q_i (i=1,2) and Γ be the interface between the two regions. Then $q(x)$ can be represented as

$$q(x) = q_1 H(\phi(x)) + q_2(1 - H(\phi(x))) \quad \text{in} \quad \Omega, \tag{3}$$

where $H(x)$ is the Heaviside function, namely

$$H(x) = 1 \quad \text{for} \quad x \geq 0 \quad ; \quad H(x) = 0 \quad \text{for} \quad x < 0,$$

and $\phi(x)$ is the level set function satisfying

$$\begin{aligned} \Omega_1 &= \{x \in \Omega \quad | \quad \phi(x) > 0\}, \\ \Omega_2 &= \{x \in \Omega \quad | \quad \phi(x) < 0\}, \\ \Gamma &= \{x \in \Omega \quad | \quad \phi(x) = 0\}. \end{aligned}$$

To determine the material interface Γ, it is suffice to determine the level set function ϕ. It is clear that many different level set functions can achieve the above requirement. We will employ a signed distance function defined by

$$\phi(x) = \begin{cases} d(x,\Gamma), & \text{if } x \in \Omega_1, \\ -d(x,\Gamma), & \text{if } x \in \Omega_2. \end{cases} \tag{4}$$

It is clear that ϕ satisfies the partial differential equation

$$|\nabla \phi| = 1, \quad \text{in} \quad \Omega. \tag{5}$$

However, ϕ is not the only solution to (5) in the sense of distribution. The unique solution to (5) is defined in the sense of viscosity solution. Let $\tilde{\phi}$ be any level set function that is positive inside Γ and negative outside Γ. Then the viscosity solution to (5) is defined as the unique steady state solution to

$$\frac{\partial d}{\partial t} + \text{sign}(d)(|\nabla d| - 1) = 0, \quad d(x,0) = \tilde{\phi}. \tag{6}$$

See Osher and Fedkiw [19] for details. We shall mention that there are some varaints of the level set methods which could avoid the use of the distance function and the Heaviside function H, see [24, 17] for some details. Applying idea from Vese and Chan [25], we can extend the level set function representation of $q(x)$ in (3) in the case where the domain Ω contains more than two materials. Hence, our method, which will be derived for two unknown conductivity values, can be easily generalized to recover more than two conductivity values and their

interfaces. The number of unknown conductivity values need not be specified, only the upper bound is needed. The redundant regions will disappear or merge with other regions during the iterative process. See also Chan and Tai [8].

Let N be the number of measurements made. For $1 \leq i \leq N$, we let $f_i(x)$ be a given function representing a known applied current density on $\partial\Omega$ and $m_i(x)$ be the corresponding measurement of the electrical potential on $\partial\Omega$. We also denote by $u_i(x,q)$ the theoretical value of the electrical potential on Ω due to $f_i(x)$, where we emphasis the dependence of u_i on $q(x)$. Since the solution to the Neumann problem (1)-(2) is not unique, we impose the following constraint on $u_i(x,q)$:

$$\int_{\partial\Omega} u_i(x,q)\, dx = 0,$$

which means a ground state potential is specified. In order to find q_1, q_2, and the location of Γ, we minimize the following functional

$$F(\phi, q_1, q_2) = \frac{1}{2}\sum_{i=1}^{N} \int_{\partial\Omega} |u_i(s,q) - m_i(s)|^2\, ds.$$

Since the minimization problem is highly ill-posed, we will introduce a regularization term in the functional. Our choise is the total variation regularization, namely, we will find the minimum of the following functional

$$F(\phi, q_1, q_2) = \frac{1}{2}\sum_{i=1}^{N} \int_{\partial\Omega} |u_i(s,q) - m_i(s)|^2\, ds + \beta \int_{\Omega} |\nabla q|\, dx \tag{7}$$

where β is a regularization parameter to be chosen and

$$\int_{\Omega} |\nabla q|\, dx$$

is the total variational norm of q (cf. Ziemer [27]). The key of our numerical scheme is that the choice of total variation regularization ensures that both the jumps of coefficient values and the lengths of interfaces are controlled. See also Vese and Osher [26]. This is different from the standard level set technique, which only controls the length.

We notice that F defined in (7) is a functional of q which again is a function of ϕ, q_1 and q_2. So, in order to compute the gradient of $F(\phi, q_1, q_2)$, we need to evaluate the derivative of F with respect to q as well as the partial derivatives of q with respect to ϕ, q_1 and q_2 respectively. The derivative of F with respect to q is given by

$$\frac{dF}{dq} = -\sum_{i=1}^{N} \nabla u_i \cdot \nabla z_i - \beta \nabla \cdot \left(\frac{\nabla q}{|\nabla q|}\right), \tag{8}$$

where z_i $(i = 1, 2, \cdots, N)$ is the solution to the following problem

$$\begin{aligned} -\nabla \cdot (q \nabla z_i) &= 0 \quad \text{in} \quad \Omega, \\ q\frac{\partial z_i}{\partial n} &= u_i - m_i \quad \text{on} \quad \partial\Omega, \end{aligned}$$

with the constraint

$$\int_{\partial\Omega} z_i(x)\, dx = 0.$$

The first term on the right hand side of (8) is the derivative with respect to q of the first term on the right hand side of (7). The proof of this part can be found in the appdenix. The second term on the right hand side of (8) is the derivative with respect to q of the second term on the right hand side of (7). For this part, we need

$$\beta|\nabla q|^{-1}\frac{\partial q}{\partial n} = 0, \quad \text{on } \partial\Omega.$$

We neglect this term since the regularization parameter β is usually chosen to be small.

By the chain rule, we have (c.f. Chan and Tai [8])

$$\frac{dF}{d\phi} = \frac{dF}{dq}\frac{dq}{d\phi} = \frac{dF}{dq}(q_1 - q_2)\delta(\phi) \tag{9}$$

$$\frac{dF}{dq_1} = \int_\Omega \frac{dF}{dq}\frac{dq}{dq_1}\, dx = \int_\Omega \frac{dF}{dq}H(\phi)\, dx. \tag{10}$$

$$\frac{dF}{dq_2} = \int_\Omega \frac{dF}{dq}\frac{dq}{dq_2}\, dx = \int_\Omega \frac{dF}{dq}(1 - H(\phi))\, dx, \tag{11}$$

where δ is the Dirac delta function.

We will use the method of gradient descent to solve the minimization problem. More precisely, we will consider the following iterative scheme for ϕ, q_1 and q_2:

$$\phi^{k+1} = \phi^k - \alpha_k \frac{dF}{d\phi}(\phi^k, q_1^k, q_2^k) \tag{12}$$

$$q_j^{k+1} = q_j^k - \gamma_k^j \frac{dF}{dq_j}(\phi^{k+1}, q_1^k, q_2^k) \quad j = 1, 2, \tag{13}$$

The step sizes $\alpha_k > 0$ and $\gamma_i^k > 0$ can be fixed during all the iterations or be obtained by line search. However, in all of the following numerical tests, we use line search for α_k and γ_k^j $(j = 1, 2)$. Precautions have to be taken when conducting numerical calculations with the delta function $\delta(\phi)$ and the Heaviside function $H(\phi)$. They are, in a more precise sense, limits of C^∞ functions. One way to tackle this problem is to replace the delta function $\delta(\phi)$ and the Heaviside function $H(\phi)$ by using the following smooth approximations

$$\delta_\epsilon(\phi) = \frac{\epsilon}{\pi(\phi^2 + \epsilon^2)}, \tag{14}$$

$$H_\epsilon(\phi) = \frac{1}{\pi}\tan^{-1}(\frac{\phi}{\epsilon}) + \frac{1}{2}, \tag{15}$$

with $\epsilon > 0$ chosen to be the order of the mesh size. See Vese and Chan [25] and Chan and Tai [8].

3 Numerical tests

This section aims at showing the usefulness of the numerical scheme derived in previous section. A series of numerical experiments was carried out in order to confirm numerically that the scheme is able to recover simutaneously the material interface and conductivity coefficient values in some situations which appear often in practice.

For ease of exposition, we set $\Omega = [0,1]^2$. We will triangulate the domain by dividing it into uniform squares with side length h. Each square is then divided into two triangles by cutting along one of its diagonals. As a result, we have a set of triangles triangulating the domain Ω. In all of the following examples, we take $h = 1/16$. Furthermore, we will always use dash lines to represent the numerical computed interface while use solid lines to represent the true interface.

The data for the potential u on the boundary is generated in the following manner. We set u equals 1 on one of the four sides of the rectangular domain Ω and 0 elsewhere. So, we have a set of 4 data in this form. Next we divide each side of Ω into two parts. Then set u equals one on one part and zero on the other part. u is also given a value of zero on the other three sides. So, we have a set of eight data in this form. Next we divide each side into four parts and set u equals one on one part and zero on the other three parts. Then, we get a set of 16 data in this form. Hence, by continuing in this manner, we have a set of 4, 12, 28 and 60 data respectively.

We will also add some noise to the data. We use the relative error in the L^2-norm on the boundary to measure the noise level in the data.

3.1 Simultaneously reconstruction

In this example, we use 60 measurement data with 0.05% noise. The regularization parameter β is chosen to be 10^{-7}. The true conductivity value is 1 inside the region enclosed by the solid line and is 10 outside. We will fix $q_2 = 10$ during the iterations. We pick a circle, showing in dash line in the left picture below, as our initial guess for the material interface. Also, we pick an initial guess for the conductivity coefficient to be 1.1 inside. The numerical result after 200 iterations is shown in Figure 1. At convergence, the conductivity is 1.3 inside.

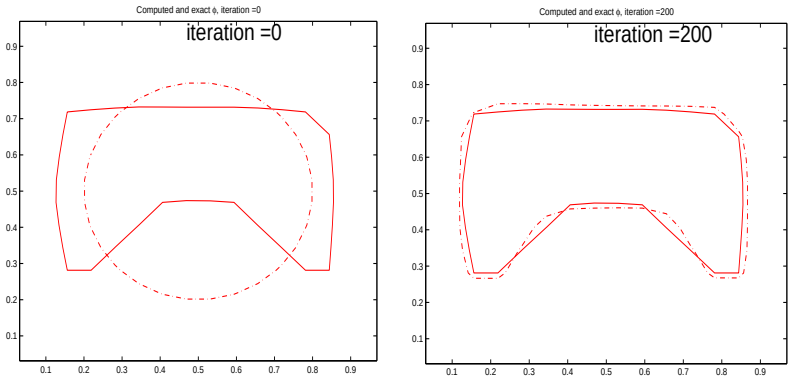

Figure 1: Left picture shows the initial guess. Right picture shows the numerical result after 200 iterations.

We see that, in the presence of 0.05% noise in the measurement data, our numerical scheme can almost recover the shape of the unknown interface. Furthermore, we see that we can recover the geometry of the unknown interface without knowing much about it, as it is seen from our choice of the initial guess which contains no information about the true interface.

Now, we will consider the same example as above but with different noise level. We add, in this case, 0.1% noise in the data. We also change the regularization paramter to 10^{-6} due to the larger noise. Figure 2 shows the numerical result after 200 iterations. The recovered value of the conductivity coefficient inside the region is 1.8.

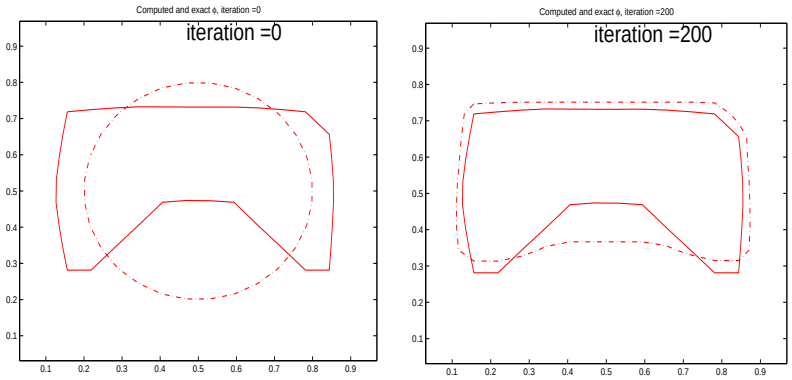

Figure 2: Left picture shows the initial guess. Right picture shows the numerical result after 200 iterations.

Now, we would consider one more example with different shape. We will again use 60 measurements. In this case, we add 0.1% noise in the data. The regularization parameter β is chosen to be 10^{-6}. The true conductivity value is again 1 inside the region enclosed by the solid line and is 10 outside. The initial

guess for the value inside the region is 1.1. Figure 3 shows the initial guess for the interface and the numerical solution of the interface at 200 iterations.

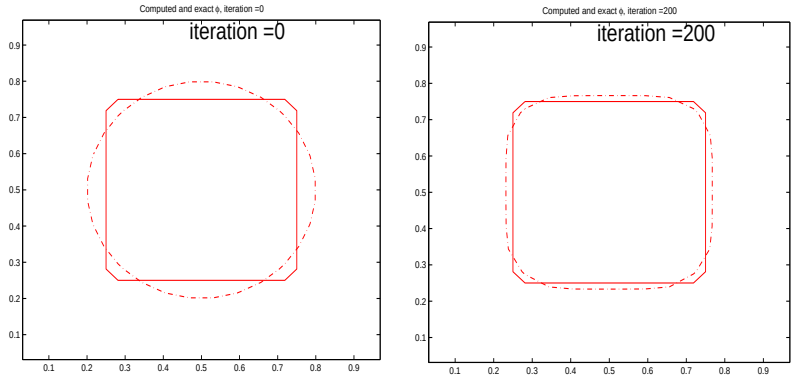

Figure 3: Left picture shows the initial guess. Right picture shows the numerical result after 200 iterations.

In this experiment, the recovered value of the conductivity inside the region is 1.3. From this numerical test, we see that our numerical algorithm can accurately recover the material interface even in the presence of 0.1% noise in the data.

In the following, we consider an example with an object with a more complicated geometry. We will first test the algorithm with no noise in the given data. We take 60 measurements and set the regularization parameter β to be 10^{-12}. We decrease the mesh size to $h = \frac{1}{32}$. The true value of the conductivity coefficient is 1 inside the region and is 10 outside the region. The initial guess for the value inside the region is 1.1. Figure 4 shows the initial guess of the interface and the numerical solution after 50000 iterations. Figure 5 shows numerical results of the same example with 0.01% noise in the data.

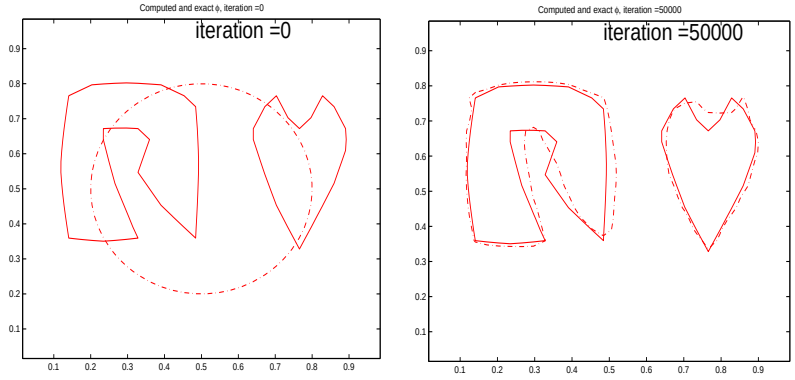

Figure 4: Results with no noise in the data. Left: initial guess. Right: numerical solution after 50000 iterations. $q = 1.789$.

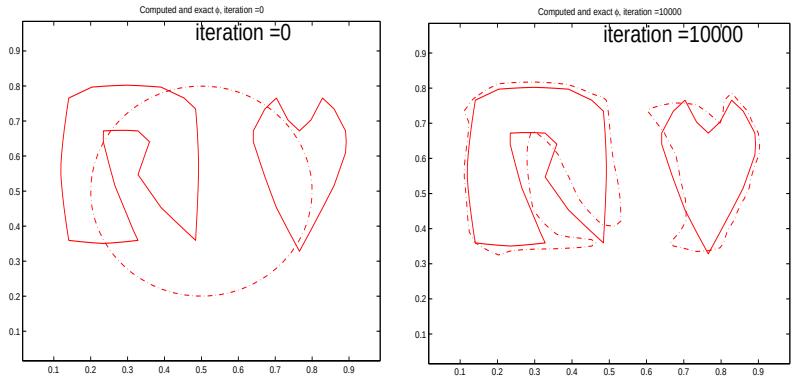

Figure 5: Results with 0.01% noise in the data. Left: initial guess. Right: numerical solution after 10000 iterations. $q = 1.941$.

In the following, we have a numerical result of the same example but with the mesh size decreased to $h = \frac{1}{64}$. From Figure 6, we see that the concave part of the object can be more accurately recovered. Moreover, the recovered value of the conductivity coefficient is more accurate.

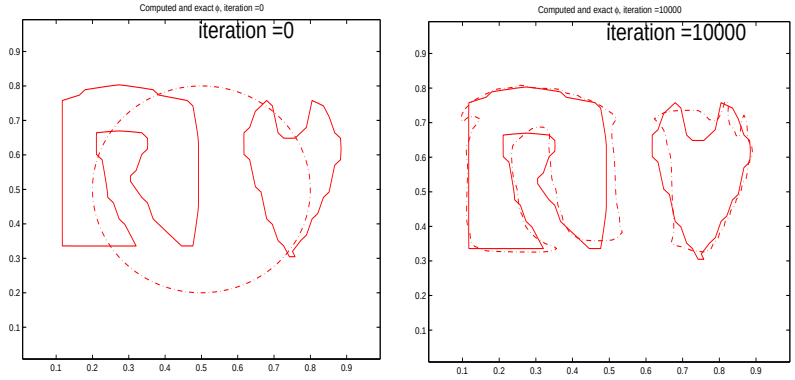

Figure 6: Result with 0.01% noise in the data. Left: initial guess. Right: numerical result after 10000 iterations. $q = 1.599$

3.2 Effect on number of observations

In this section, we will see the effect of the number of observations on the accuracy of the numerical solution. Here, we take the regularization parameter β to be 10^{-8} and we also add 1% noise in the data. To see the effect, we perform four different numerical calculations of a known interface by using 4, 12, 28 and 60 measurements. Figure 7 shows an initial guess for our method. The numerical results are shown in the Figure 8. The upper left, upper right, lower left and lower right figures show results with 4, 12, 28 and 60 measurements respectively. From the numerical results above, we see that, as the number of

measurements increases, we have a better accuracy of the unknown interface. When the number of measurement is 60, we almost recover the exact interface. In addition, when the number of measurement is 4, we still roughly get the shape of the unknown interface. From this numerical experiment, we see that the concave portion of the unknown object is more difficult to be recovered than other part where the object is convex.

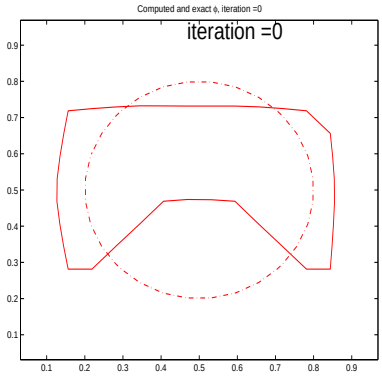

Figure 7: A circle is chosen to be an initial guess.

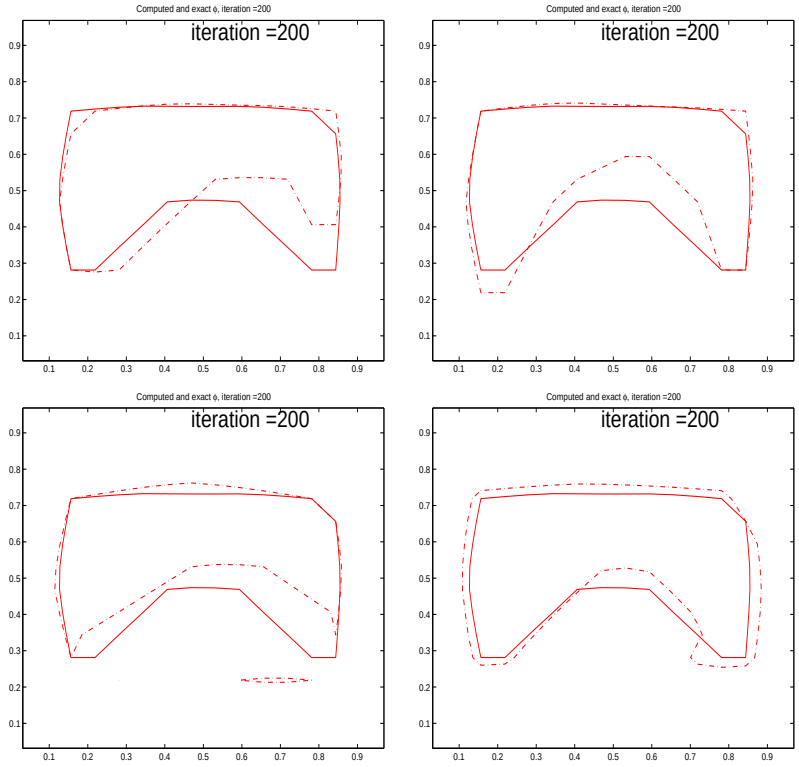

Figure 8: The upper left, upper right, lower left and lower right figures show results with 4, 12, 28 and 60 measurements.

3.3 Effect on noise level

In this section, we will see the effect of the noise on the computational results. We will test our algorithm against different noise levels. Here we fix the regularization parameter β to be 10^{-5} and the number of measurements to be 60. We will perform four numerical tests with noise ranging from 1% to 4%. The true interface in this case is a square sitting in the middle of the domain Ω. We pick an initial guess for the numerical scheme to be a circle sitting in the middle of the domain. In Figure 10, we show the numerically computed interfaces with different noise levels. The upper left, upper right, lower left and lower right figures show the numerically computed interface with 1%, 2%, 3% and 4% of noise in the data respectively. We see that our numerical algorithm can tolerate noise level up to 3%. Also, at this noise level, our algorithm can produce quite accurate result. However, our scheme fails for this rectangular object in the presence of 4% noise in the data.

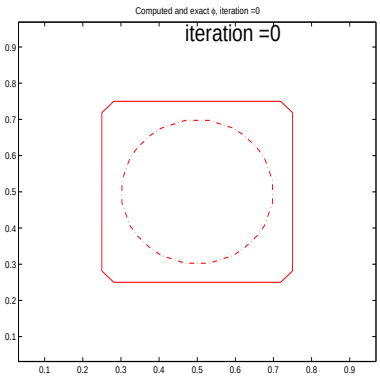

Figure 9: A circle is chosen to be an initial guess.

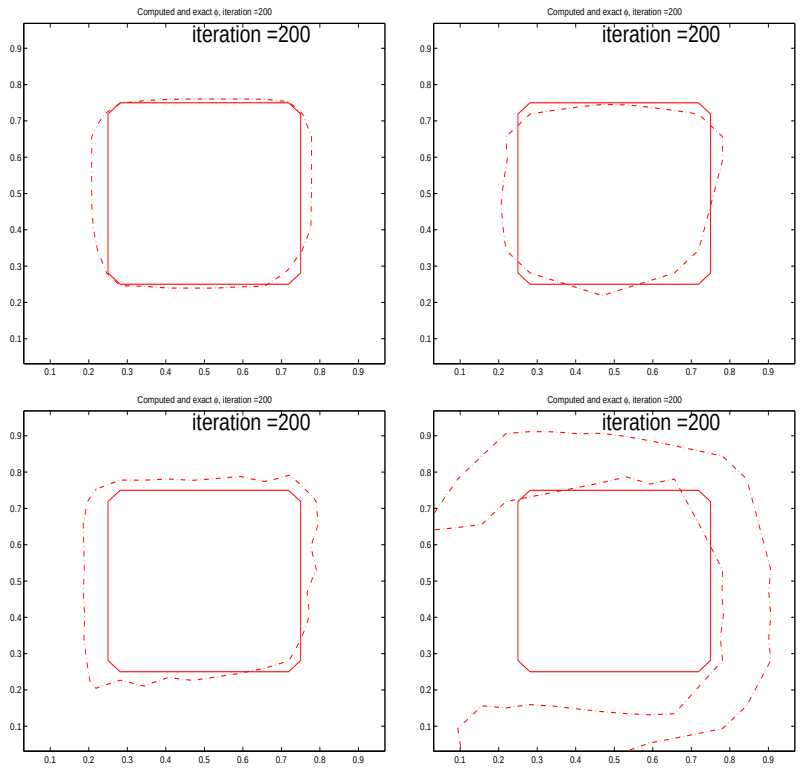

Figure 10: The upper left, upper right, lower left and lower right figures show results with 1%, 2%, 3% and 4% noise resepectively.

3.4 Effect on regularization parameter

In this section, we will demonstrate the effect of the choice of the regularization parameter β. We fix the number of measurements to be 60 and the noise level to be 1%. The true interface is a circle sitting in the middle of the domain. The initial guess is chosen to be a circle with the same center as that of the true interface and smaller radius.

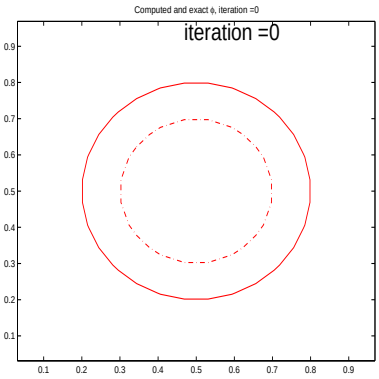

Figure 11: A circle is chosen to be an initial guess.

We show the results with different regularization parameters in Figure 12. The upper left, upper right, lower left and lower right figures show the results with the regularization parameter is chosen to be 10^{-4}, 10^{-5}, 10^{-6} and 10^{-7} respectively. From this numerical experiment, we see that the choice of the regularization parameter is cruical to the success of our numerical scheme. When the regularization parameter is 10^{-4}, the numerical interface is far away from the exact interface. When the regularization is 10^{-6} or 10^{-7}, we see that the numerical solution of the interface has some corners and so they are not giving a good result for the unknown interface. In this particalar example, we claim that a good choice of the regularization parameter would be 10^{-5}.

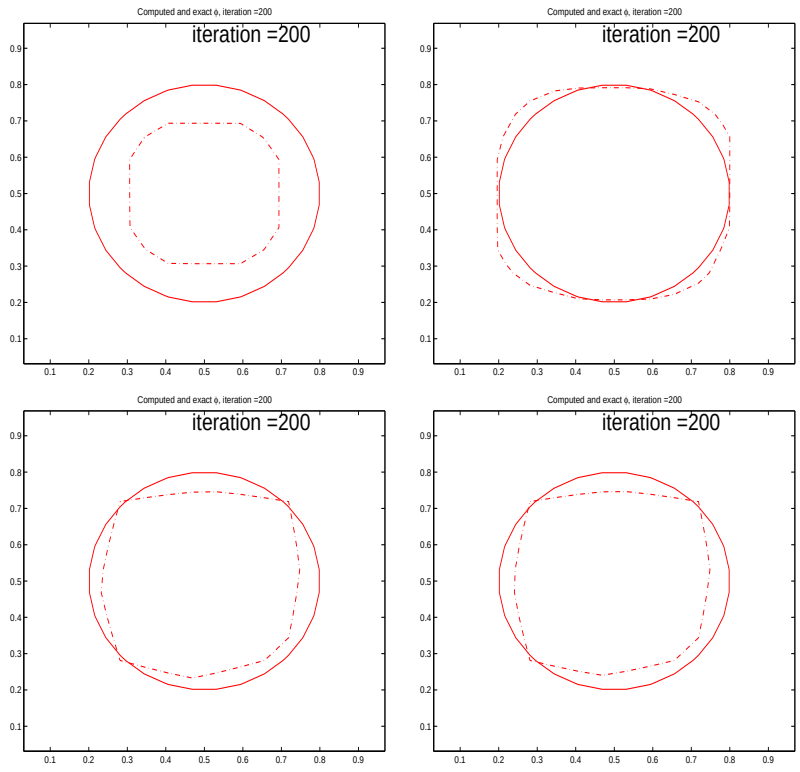

Figure 12: The upper left, upper right, lower left and lower right figures show results with the regularization parameter chosen to be 10^{-4}, 10^{-5}, 10^{-6} and 10^{-7} respectively.

4 Conclusion

For eletrical impedance tomography, it is sometimes more important to recover the shape of the domains containing different materials than to recver the values for the materials. Level set methods are natural choices for this kind of applications. In this work, we have demonstrated that level set methods can produce rather good results in identifying the sharp interfaces in the presence of noise in the observation data. In order use this approach for practical problems, we need to improve the efficiency of the algorithms. More efficient level set minimization algorithms shall be tested [24]. An efficient algorithm for solving the forward problems would also improve a lot of the numerical performances of the proposed algorithms.

5 Appendix: computation of gradient

In this section, we will give a derivation of the gradient used in (8). The result here is rather standard and can be found in standard text. We include this section for completeness.

Fix $q(x) \in L^\infty(\Omega)$ with $q(x) > q_0 > 0$. Define a function space

$$X := \{u \in H^1(\Omega) \mid \int_\Omega u \, dx = 0\},$$

with an inner product

$$< u, v >_X := \int_\Omega q \nabla u \cdot \nabla v \, dx,$$

and norm $\|u\|_X :=< u, u >_X^{\frac{1}{2}}$. By virtue of the Poincare's inequality:

$$\|u\|_{L^2(\Omega)} \leq K \|\nabla u\|_{L^2(\Omega)} \quad \text{for all} \quad u \in X,$$

the space X is a Hilbert space with a norm which is equivalent to the standard H^1-norm.

Fix $\eta(x) \in L^\infty(\Omega)$ with $\eta(x) > \eta_0 > 0$. Our task is to compute the Gateaux derivative of F with respect to q in the η direction, that is, we want to prove the following

$$\frac{\partial F}{\partial q} \cdot \eta = \sum_{i=1}^{N} \int_{\partial\Omega} (u_i(s,q) - m_i(s)) \frac{\partial u_i}{\partial q} \cdot \eta \, ds.$$

In order to compute the Gateaux derivative of u_i $(1 \leq i \leq N)$ with respect to q, we consider the following problem

$$-\nabla \cdot ((q + \epsilon\eta)\nabla u_\epsilon) = 0 \quad \text{in} \quad \Omega, \tag{16}$$

$$(q + \epsilon\eta)\frac{\partial u_\epsilon}{\partial n} = f \quad \text{on} \quad \partial\Omega. \tag{17}$$

Lemma 1 *There exist $\epsilon_0 > 0$ depending only on q and η such that u_ϵ is uniformly bounded in X for $-\epsilon_0 < \epsilon < \epsilon_0$.*

Proof. Multiplying both sides of (16) by u_ϵ and integrating on Ω, we have

$$\int_\Omega (q + \epsilon\eta)|\nabla u_\epsilon|^2 \, dx = \int_{\partial\Omega} f u_\epsilon \, ds.$$

By Cauchy Schwarz inequality and trace theorem,

$$\int_{\partial\Omega} f u_\epsilon \, ds \leq \|f\|_{L^2(\partial\Omega)} \|u_\epsilon\|_{L^2(\partial\Omega)} \leq K \|f\|_{L^2(\partial\Omega)} \|u_\epsilon\|_X,$$

where the last inequality follows from the fact that X-norm is equivalent to H^1-norm. If $\epsilon \geq 0$, we always have

$$q + \epsilon\eta > q_0 > \frac{q_0}{2}.$$

If $\epsilon < 0$, we pick ϵ small enough such that

$$q + \epsilon\eta \geq q_0 + \epsilon\|\eta\|_{L^\infty(\Omega)} > \frac{q_0}{2}$$

which means $\epsilon > -q_0(2\|\eta\|_{L^\infty(\Omega)})^{-1}$. By choosing $\epsilon_0 := q_0(2\|\eta\|_{L^\infty(\Omega)})^{-1}$, we have

$$\frac{q_0}{2}\int_\Omega |\nabla u_\epsilon|^2\, dx \leq \int_\Omega (q+\epsilon\eta)|\nabla u_\epsilon|^2\, dx,$$

for $-\epsilon_0 < \epsilon < \epsilon_0$. Hence, the lemma follows.

□

Let v be any function in X. Multiplying both sides of (1) by v and integrating both sides on Ω, we obtain

$$\int_\Omega q\nabla u \cdot \nabla v\, dx - \int_{\partial\Omega} fv\, ds = 0. \tag{18}$$

Similarly, from (16), we obtain

$$\int_\Omega (q+\epsilon\eta)\nabla u_\epsilon \cdot \nabla v\, dx - \int_{\partial\Omega} fv\, ds = 0. \tag{19}$$

Combining (18) and (19), we get

$$\int_\Omega q(\nabla u_\epsilon - \nabla u)\cdot\nabla v\, dx + \epsilon\int_\Omega \eta\nabla u_\epsilon\cdot\nabla v\, dx = 0. \tag{20}$$

Lemma 2 *We have*

$$u_\epsilon \to u \quad \text{strongly in} \quad X \quad \text{as} \quad \epsilon \to 0. \tag{21}$$

Proof. Putting $v = u_\epsilon - u$ in (20), we have,

$$\int_\Omega q|\nabla(u_\epsilon - u)|^2\, dx + \epsilon\int_\Omega \eta\nabla u_\epsilon\cdot\nabla(u_\epsilon - u)\, dx = 0.$$

Notice that

$$\int_\Omega \eta\nabla u_\epsilon\cdot\nabla(u_\epsilon - u)\, dx \leq K\|u_\epsilon\|_X\|u_\epsilon - u\|_X,$$

with K depends on q and η. Since u_ϵ is uniformly bounded in X for $-\epsilon_0 < \epsilon < \epsilon_0$, we have

$$\lim_{\epsilon\to 0}\int_\Omega q|\nabla(u_\epsilon - u)|^2\, dx = 0.$$

□

Consequently, for all $v \in X$, we have

$$\lim_{\epsilon \to 0} \int_\Omega \eta \nabla u_\epsilon \cdot \nabla v \, dx = \int_\Omega \eta \nabla u \cdot \nabla v \, dx. \tag{22}$$

Dividing both sides of (20) by ϵ, we have

$$\int_\Omega q \nabla (\frac{u_\epsilon - u}{\epsilon}) \cdot \nabla v \, dx = - \int_\Omega \eta \nabla u_\epsilon \cdot \nabla v \, dx. \tag{23}$$

In the following lemma, we will prove the family of functions $\frac{u_\epsilon - u}{\epsilon}$ converges weakly in X. Because of this fact, we define the limit to be $\frac{\partial u}{\partial q} \cdot \eta$.

Lemma 3 *We have*

$$\frac{u_\epsilon - u}{\epsilon} \to \frac{\partial u}{\partial q} \cdot \eta \quad \text{weakly as} \quad \epsilon \to 0.$$

Proof. Putting $v = \frac{u_\epsilon - u}{\epsilon}$ in (23), we have

$$\int_\Omega q \nabla (\frac{u_\epsilon - u}{\epsilon}) \cdot \nabla (\frac{u_\epsilon - u}{\epsilon}) \, dx = - \int_\Omega \eta \nabla u_\epsilon \cdot \nabla (\frac{u_\epsilon - u}{\epsilon}) \, dx.$$

Hence, for $-\epsilon_0 < \epsilon < \epsilon_0$,

$$\int_\Omega q |\nabla (\frac{u_\epsilon - u}{\epsilon})|^2 \, dx$$

is uniformly bounded in X. Then, the lemma follows from the fact that X is a Hilbert space.

□

In the following lemma, we show that we actually have strong convergence.

Lemma 4 *We have*

$$\frac{u_\epsilon - u}{\epsilon} \to \frac{\partial u}{\partial q} \quad \text{strongly as} \quad \epsilon \to 0.$$

Proof. By (23), we have

$$\begin{aligned}
&\int_\Omega q \nabla (\frac{u_\epsilon - u}{\epsilon}) \cdot \nabla (\frac{u_\epsilon - u}{\epsilon}) \, dx \\
&= - \int_\Omega \eta \nabla u_\epsilon \cdot \nabla (\frac{u_\epsilon - u}{\epsilon}) \, dx \\
&= - \int_\Omega \eta \nabla u \cdot \nabla (\frac{u_\epsilon - u}{\epsilon}) \, dx + \int_\Omega \eta \nabla (u - u_\epsilon) \cdot \nabla (\frac{u_\epsilon - u}{\epsilon}) \, dx.
\end{aligned}$$

The second term in the last expression tends to zero as $\epsilon \to 0$ since

$$\int_\Omega \eta \nabla (u - u_\epsilon) \cdot \nabla (\frac{u_\epsilon - u}{\epsilon}) \, dx = \epsilon \int_\Omega \eta \nabla (\frac{u_\epsilon - u}{\epsilon}) \cdot \nabla (\frac{u_\epsilon - u}{\epsilon}) \, dx.$$

For the first term, by weak convergence, we have

$$\lim_{\epsilon\to 0} -\int_\Omega \eta\nabla u\cdot\nabla(\frac{u_\epsilon-u}{\epsilon})\,dx = -\int_\Omega \eta\nabla u\cdot\nabla(\frac{\partial u}{\partial q}\cdot\eta)\,dx.$$

From (22) and (23), we have

$$\int_\Omega q\nabla(\frac{\partial u}{\partial q}\cdot\eta)\cdot\nabla(\frac{\partial u}{\partial q}\cdot\eta)\,dx = -\int_\Omega \eta\nabla u\cdot\nabla(\frac{\partial u}{\partial q}\cdot\eta)\,dx.$$

Combining the results, we obtain

$$\lim_{\epsilon\to 0}\|\frac{u_\epsilon-u}{\epsilon}\|_X = \|\frac{\partial u}{\partial q}\cdot\eta\|_X,$$

which proves the lemma.

□

The following lemma gives the formula for the Gateaux derivative of F with respect to q in the η direction.

Lemma 5 *We have*

$$\frac{\partial F}{\partial q}\cdot\eta = \sum_{i=1}^N\int_{\partial\Omega}(u_i(s,q)-m_i(s))\frac{\partial u_i}{\partial q}\cdot\eta\,ds.$$

Proof. Notice that

$$\begin{aligned}
&F(q+\epsilon\eta)-F(q)\\
=&\frac{1}{2}\sum_{i=1}^N\int_{\partial\Omega}\left\{(u_i(s,q+\epsilon\eta)-m_i(s))^2-(u_i(s,q)-m_i(s))^2\right\}ds\\
=&\frac{1}{2}\sum_{i=1}^N\int_{\partial\Omega}|u_i(s,q+\epsilon\eta)-u_i(s,q)|^2\,ds\\
&+\sum_{i=1}^N\int_{\partial\Omega}(u_i(s,q+\epsilon\eta)-u_i(s,q))(u_i(s,q)-m_i(s))\,ds.
\end{aligned}$$

So, we have

$$\begin{aligned}
&\frac{F(q+\epsilon\eta)-F(q)}{\epsilon}\\
=&\frac{\epsilon}{2}\sum_{i=1}^N\int_{\partial\Omega}|\frac{u_i(s,q+\epsilon\eta)-u_i(s,q)}{\epsilon}|^2\,ds\\
&+\sum_{i=1}^N\int_{\partial\Omega}(\frac{u_i(s,q+\epsilon\eta)-u_i(s,q)}{\epsilon})(u_i(s,q)-m_i(s))\,ds.
\end{aligned}$$

For each $i = 1, 2, \cdots, N$,

$$\begin{aligned}
&\int_{\partial\Omega} \left(\frac{u_i(s, q+\epsilon\eta) - u_i(s,q)}{\epsilon} - \frac{\partial u_i}{\partial q}\cdot\eta\right)(u_i(s,q) - m_i(s))\, ds \\
\leq &\left\|\frac{u_i(s, q+\epsilon\eta) - u_i(s,q)}{\epsilon} - \frac{\partial u_i}{\partial q}\cdot\eta\right\|_{L^2(\partial\Omega)} \|u_i(s,q) - m_i(s)\|_{L^2(\partial\Omega)} \\
\leq &\left\|\frac{u_i(s, q+\epsilon\eta) - u_i(s,q)}{\epsilon} - \frac{\partial u_i}{\partial q}\cdot\eta\right\|_{X} \|u_i(s,q) - m_i(s)\|_{L^2(\partial\Omega)} \\
\to &0 \quad \text{as} \quad \epsilon \to 0.
\end{aligned}$$

Hence, we obtain

$$\lim_{\epsilon\to 0} \frac{F(q+\epsilon\eta) - F(q)}{\epsilon} = \sum_{i=1}^{N} \int_{\partial\Omega} (u_i(s,q) - m_i(s)) \frac{\partial u_i}{\partial q}\cdot\eta\, ds.$$

□

Fix i with $1 \leq i \leq N$. Consider the following variational problem: find $z_i \in X$ such that

$$\int_\Omega q\nabla z_i \cdot \nabla w\, dx = \int_{\partial\Omega} (u_i(s,q) - m_i(s)) w\, ds, \tag{24}$$

for all $w \in X$. By Lax-Milgram theorem, it has a unique solution. Putting $w = \frac{\partial u_i}{\partial q}\cdot\eta$, we have

$$\int_\Omega q\nabla z_i \cdot \nabla\left(\frac{\partial u_i}{\partial q}\cdot\eta\right) dx = \int_{\partial\Omega} (u_i(s,q) - m_i(s)) \frac{\partial u_i}{\partial q}\cdot\eta\, ds. \tag{25}$$

From (22) and (23), we have

$$\int_\Omega q\nabla z_i \cdot \nabla\left(\frac{\partial u_i}{\partial q}\cdot\eta\right) dx = -\int_\Omega \eta\nabla z_i \cdot \nabla u_i\, dx.$$

Summing (25) from $i = 1$ to $i = N$, we have

$$\frac{\partial F}{\partial q}\cdot\eta = -\eta \sum_{i=1}^{N} \int_\Omega \nabla z_i \cdot \nabla u_i\, dx.$$

Consequently, we prove the following

Theorem 1 *We have*

$$\frac{\partial F}{\partial q} = -\sum_{i=1}^{N} \nabla z_i \cdot \nabla u_i. \tag{26}$$

References

[1] Andrew Allers and Fadil Santosa. Stability and resolution analysis of a linearized problem in electrical impedance tomography. *Inverse Problems*, 7(4):515–533, 1991.

[2] Hend Ben Ameur, Martin Burger, and Benjamin Hackl. On some geometric inverse problems in linear elasticity. *UCLA, Math. Depart., CAM-report 03-35*, 2003.

[3] Martin Brühl. *Explicit characterization of inclusions in electrical impedance tomography.* SIAM J. Math. Anal., 32 (2001), pp. 1327-1341.

[4] Martin Brühl and Martin Hanke. *Numerical implementation of two non-iterative methods for locating inclusions by impedance tomography.* Inverse Problems, 16 (2000), pp. 1029-1042.

[5] Martin Burger. A level set method for inverse problems. *Inverse problems*, 17:1327–1356, 2001.

[6] Martin Burger. Levenberg-marquardt level set methods for inverse obstacle problems. *UCLA, Math. Depart., CAM-report 03-45*, 2003.

[7] Martin Burger. *A framework for the construction of level set methods for shape optimization and reconstruction.* Interfaces and Free Boundaries, 5 (2003), pp. 301-329.

[8] Tony F. Chan and Xue-Cheng Tai. *Level set and total variation regularization for elliptic inverse problems with discontinuous coefficients.* To appear in J. Comput. Phys.

[9] Tony F. Chan and Xue-Cheng Tai. *Identification of Discontinuous Coefficients from Elliptic Problems Using Total Variation Regularization.* To appear in SIAM J. Sci. Comp.

[10] Margaret Cheney, David Isaacson and Johathan C. Newell. *Electrical impedance tomography.* SIAM Rev., 41 (1999), pp 85-101 (electronic).

[11] M. Cheney, D. Isaacson, J. Newell, J. Goble and S. Simske. *NOSER: an algorithm for solving the inverse conductivity problem.* Internat. J. Imaging Systems and Technology, 2 (1990), pp. 66-75.

[12] David C. Dobson and Fadil Santosa. An image-enhancement technique for electrical impedance tomography. *Inverse Problems*, 10(2):317–334, 1994.

[13] David C. Dobson and Fadil Santosa. Resolution and stability analysis of an inverse problem in electrical impedance tomography: dependence on the input current patterns. *SIAM J. Appl. Math.*, 54(6):1542–1560, 1994.

[14] D. C. Dobson and F. Santosa, *An image enhancement technique for eletrical impedance tomography*, Inverse problems, 10 (1994), pp. 317–334.

[15] O. Dorn, E. L. Miller and C. M. Rappaport. *A shape reconstruction method for electromagnetic tomography using adjoint fields and level sets*. Technical report.

[16] Kazufumi Ito, Karl Kunisch and Zhilin Li. *Level-set function approach to an inverse interface problem*. Inverse Problems, 17 (2001), pp. 1225-1242.

[17] Johan Lie, Marius Lysaker and Xue-Cheng Tai. . A Variant of the Level Set Method and Applications to Image Segmentation. *UCLA CAM report 03-50*, 2003. Available online at: http://www.math.ucla.edu/applied/cam.

[18] Stanley J. Osher Martin Burger and Eli Yablonovitch. Inverse problem techniques for the design of photonic crystals. *UCLA, Math. Depart., CAM-report 03-31*, 2003.

[19] Stanley J. Osher and Ronald R. Fedkiw. *Level set methods*. CAM Report 00-08, UCLA Math. Dept., Feb. 2000.

[20] Stanley J. Osher and Fadil Santosa. *Level set methods for optimization problems involving geometry and constraints. I. Frequencies of a two-density inhomogeneous drum*. J. Comput. Phys., 171 (2001), pp. 272-288.

[21] Stanley J. Osher and James A. Sethian. *Fronts propagating with curvature dependent speed: algorithms based on hamilton-jacobi formulations*. J. Comput. Phys., 79 (1988), pp. 12-49.

[22] L. Rondi and F. Santosa. *Enchanced electrical impedance tomography via the Mumford-Shah functional*. Preprint.

[23] Fadil Santosa and Michael Vogelius. A backprojection algorithm for electrical impedance imaging. *SIAM J. Appl. Math.*, 50(1):216–243, 1990.

[24] B. Song and T.F. Chan. Fast algorithm for level set segmentation. *UCLA CAM report 02-68*, 2002.

[25] Luminita A. Vese and Tony F. Chan. *A new multiphase level set framework for image segmentation via the Mumford and Shah model*. CAM Report 01-25, UCLA Math. Dept., April 2001.

[26] L. Vese and S. Osher. *The level set method links active contours, Mumford-Shah segmentation, and total variation restoration*. CAM Reoirt 02-05, UCLA Math. Dept., 2002.

[27] W. P. Ziemer. *Weakly differentiable functions*. Springer-Verlag, 1989.